Geophysical Prospecting

EAGE EUROPEAN ASSOCIATION OF GEOSCIENTISTS & ENGINEERS

Geophysical Prospecting, 2016 doi: 10.1111/1365-2478.12375

Validation of the boundary conditions to model the seismic response of fractures

Robiel Martinez Corredor[1]*, Juan E. Santos[2,5], Patricia M. Gauzellino[3] and José M. Carcione[4]

[1]*Facultad de Ingeniería, Universidad Nacional de La Plata, Calle 1 y 47, La Plata (B1900TAG), Pcia. de Buenos Aires, Argentina,* [2]*Instituto del Gas y del Petróleo, Facultad de Ingeniería, Universidad de Buenos Aires, CONICET, Av. Las Heras 2214 Piso 3, C1127AAR, Buenos Aires, Argentina,* [3]*Departamento de Geofísica Aplicada, Facultad de Ciencias Astronómicas y Geofísicas, Universidad Nacional de La Plata, Paseo del Bosque s/n, La Plata, B1900FWA, Argentina,* [4]*Istituto Nazionale di Oceanografia e di Geofisica Sperimentale (OGS), Borgo Grotta Gigante 42c, 34010 Sgonico, Trieste, Italy, and* [5]*Department of Mathematics, Purdue University, 150 N. University Street, West Lafayette, Indiana, 47907-2067 USA*

Received November 2014, revision accepted February 2016

ABSTRACT

Fractures in fluid-saturated poroelastic media can be modeled as extremely thin, highly permeable, and compliant layers or by means of suitable boundary conditions that approximate the behavior of such thin layers. Since fracture apertures can be very small, the numerical simulations would require the use of extremely fine computational meshes and the use of boundary conditions would be required.

In this work, we study the validity of using boundary conditions to describe the seismic response of fractures. For this purpose, we compare the corresponding scattering coefficients to those obtained from a thin-layer representation. The boundary conditions are defined in terms of fracture apertures that, in the most general case, impose discontinuity of displacements, fluid pressures, and stresses across a fracture. Furthermore, discontinuities of either fluid pressures, stresses, or both can be removed, or displacement jumps proportional to the stresses and/or pressures can be expressed via shear and normal dry compliances in order to simplify.

In the examples, we vary the permeability, thickness, and porosity of the fracture and the type of fluid saturating the background medium and fractures. We observe good agreement of the scattering coefficients in the seismic range obtained with the two different approaches.

1 INTRODUCTION

Seismic wave propagation in fractured media is an active area of research, with applications in many fields such as hydrocarbon geophysics exploration, seismic monitoring of reservoir production, and mining among others. The modelling of fractures may be considered a special case of the thin-layer problem, where the fracture is represented by a very thin layer with high permeability and compliance (see Daley 2006; Kong *et al.* 2013; Lambert, Gurevich, and Brajanovski 2005; Nakagawa and Schoenberg 2007) among others.

There is a large number of works for a layer described by a single-phase (solid) case. For example, Widess (1973) and Bakke and Ursin (1998) considered the normal incidence case for a thin layer and Juhlin and Young (1993) studied amplitude-versus-offset effects of a thin layer, whereas the effect of the thickness of a sedimentary layer was investigated by Chung and Lawton (1995, 1996). Carcione (2001) computed the scattering response of a lossy layer having orthorhombic symmetry and embedded between two isotropic half-spaces, and Liu and Schmitt (2003) obtained the P-wave

*E-mail: robielmartinez@yahoo.com

reflection coefficient in isotropic lossless thin layer as a function of the incidence angle.

Several theories have appeared in the literature to model fractures by applying specific boundary conditions in the context of wave propagation phenomena. The linear-slip interface model (non-welded) for flat viscoelastic 2D fractures was proposed by Schoenberg (1980). This model imposes the continuity of the stresses and discontinuity of the displacements across the fracture. This model has been validated by laboratory experiments (Gu *et al.* 1996; Hsu and Schoenberg 1993; Pyrak-Nolte *et al.* 1990). The earlier studies considered the propagation of compressional and shear pulses in dry and wet fractured samples, and validated the linear slip theory. Moreover, Molotkov and Bakulin (1997) assumed thin fractures as an elastic medium to be very soft, in comparison with the frame.

Concerning wave propagation in fractured fluid-saturated poroelastic media, we denote the boundary conditions given by Bakulin and Molotkov (1997) and later by Nakagawa and Schoenberg (2007). In the latter work, several boundary conditions are developed, and the corresponding reflection and transmission (R–T) coefficients are computed and analysed. These boundary conditions first consider the most general case in which stresses, velocities, and fluid pressure may be discontinuous across a fracture, and later several simplified hypothesis lead to other forms of the boundary conditions, one of which reduces to that of Bakulin and Molotkov (1997).

In numerical simulations, modeling fractures as very thin layers would require the use of extremely fine computational meshes, and consequently, boundary conditions become a necessity. In this paper, we determine the frequency range in which the various boundary conditions given by Nakagawa and Schoenberg (2007) are valid to represent fractures in numerical simulation of waves in fractured poroelastic media. For this purpose, we compare the R–T coefficients of waves arriving to a plane fracture within a fluid-saturated porous medium represented either as a thin layer or as boundary conditions.

The calculation of the R-T coefficients for poroelastic media considering two interfaces is presented in the work of Wu, Xue, and Adler (1990), where the system is composed of a fluid-saturated porous solid plate immersed in fluid, and the results are compared with experimental data, and in those of Johnson, Koplik and Dashen (1994), Jocker and Smeulders (2009), and Fellah *et al.* (2013), where ultrasonic measurements are compared with numerical calculations in poroelastic slabs.

The calculation of the R–T coefficients at a very thin poroelastic layer separating two poroelastic half-spaces has been performed by Martinez *et al.* (2014). The results have been validated against limiting cases (elastic solid and inviscid fluids and zero layer thickness) and predict all the wave conversions, critical angles, and polarity changes.

In this work, we propose to use boundary conditions to model the seismic response of fractures. To validate the approach, we compare the scattering coefficients to those obtained with a thin layer. In the case of fractures represented as thin layers, the displacement fields are recast in terms of potentials, and the boundary conditions at the two interfaces impose continuity of the solid and fluid displacements, normal and shear stresses, and fluid pressure. The methodology is analogous to that presented by Santos *et al.* (1992), Rubino, Ravazzoli, and Santos (2006) and Carcione (2001, 2015). The results are verified for specific limiting cases with already published theoretical equations (Brekhovskikh 1980; Carcione 2015; Liu and Schmitt 2003; Pilant 1979; Santos *et al.* 1992). The problem is solved for all angles of incidence and a wide range of frequencies examining the effects of varying fracture porosity and different saturant fluids.

This paper is organized as follows. Biot's theory is reviewed first. Then, we present the calculation of the R–T coefficients at a fracture separating two half-spaces, with the fracture represented first as a thin layer and then using three different boundary conditions approximating the acoustic response of such layer. Next, we compare the R–T coefficients for various cases (the different boundary conditions given by Nakagawa and Schoenberg (2007) and particular fluids within the fracture) and analyse their behavior as a function of frequency and incidence angle. We analyse the frequency range in which the R–T coefficients coincide for all approaches to represent fractures.

2 BIOT'S THEORY

We consider that both the background and fracture can be described as Biot medium, i.e., a porous solid saturated by a viscous compressible fluid, and assume that the whole aggregate is isotropic. Let $\mathbf{U}$ and $\mathbf{U}_f$ be the averaged displacement vectors of the solid and fluid parts of the medium, respectively, and let the averaged relative fluid displacement per unit volume of bulk material $\mathbf{W}$ be defined as

$$\mathbf{W} = \phi\left(\mathbf{U}_f - \mathbf{U}\right), \tag{1}$$

where ϕ is the porosity.

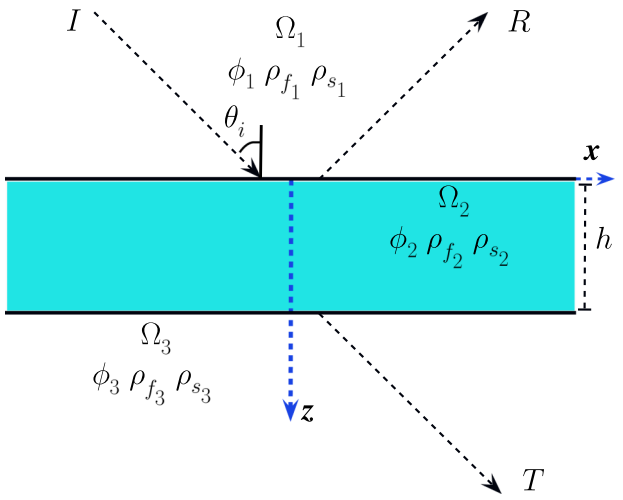

Figure 1 Geometry of the two half-spaces and the embedded thin layer.

Table 1 Material properties of the frame

Properties	Matrix	Fracture
Porosity	0.15	0.5 (case 1,2-1,2-2,3) 0.3,0.5,0.7 (case 2-3)
Solid density (g/cm^3)	2.7	2.7
Solid bulk modulus (GPa)	36	36
Frame bulk modulus (GPa)	9	0.0556
Frame shear modulus (GPa)	7	0.0333
Permeability (D)	0.1	100, 0.0001 (case 1) 0.000001 to ∞ (case 2-1) 1.0 (case 2-2,2-3) 100 (case 3)
Tortuosity	3	1

Table 2 Fluid properties

Properties	Gas	Water	Oil
Density (g/m^3)	0.1398	1	0.7
Fluid viscosity (Pa s)	0.000022	0.001	0.004
Fluid bulk modulus (GPa)	0.05543	2.25	0.57

Let ε_{ij} and σ_{ij} and P_f denote the strain and stress tensors, and fluid pressure respectively. Following Biot (1956, 1962), the stress–strain relations can be written as

$$\sigma_{ij} = 2\mu\varepsilon_{ij}(\mathbf{U}) + \delta_{ij}\left(\lambda_c \nabla\cdot\mathbf{U} + D\nabla\cdot\mathbf{W}\right), \quad i,j = 1,2,3,$$
$$P_f = -D\nabla\cdot\mathbf{U} - M\nabla\cdot\mathbf{W} \tag{2}$$

where λ_c and μ are the Lamé of the saturated rock. The grains are characterized by the density ρ_s, the bulk modulus K_s, and the shear modulus μ_s, whereas the fluid is described by ρ_f, K_f, and viscosity η. The grains compose an elastic porous matrix with porosity ϕ, permeability κ, bulk modulus K_m, and shear modulus μ_m. The constants λ_c, D, and M in equation (2) can be written as (Carcione 2015)

$$\alpha = 1 - \frac{K_m}{K_s}, \quad M = \left(\frac{\alpha-\phi}{K_s} + \frac{\phi}{K_f}\right)^{-1}, \quad D = \alpha M,$$
$$K_c = K_m + \alpha^2 M, \quad \lambda_c = K_c - \frac{2}{3}\mu, \tag{3}$$

where K_c is the undrained bulk modulus.

Then, Biot's equations of motion can be stated as:

$$\begin{aligned}\nabla\cdot\sigma &= H_c\nabla(\nabla\cdot\mathbf{U}) - \mu\nabla\times(\nabla\times\mathbf{U}) + D\nabla(\nabla\cdot\mathbf{W})\\ &= \rho_b\frac{\partial^2\mathbf{U}}{\partial t^2} + \rho_f\frac{\partial^2\mathbf{W}}{\partial t^2},\end{aligned}$$
$$\begin{aligned}-\nabla P_f &= D\nabla(\nabla\cdot\mathbf{U}) + M\nabla(\nabla\cdot\mathbf{W})\\ &= \rho_f\frac{\partial^2\mathbf{U}}{\partial t^2} + g\frac{\partial^2\mathbf{W}}{\partial t^2} + b\frac{\partial\mathbf{W}}{\partial t},\end{aligned} \tag{4}$$

where $H_c = \lambda_c + 2\mu$ and $\rho_b = (1-\phi)\rho_s + \phi\rho_f$ is the mass density of the bulk material.

The mass and viscous coupling coefficients between the solid and fluid phases are denoted by g and b (Berryman 1980, 1982):

$$g = \frac{S\rho_f}{\phi}, \quad b = \frac{\eta}{\kappa}, \quad S = \frac{1}{2}\left(1 + \frac{1}{\phi}\right), \tag{5}$$

with S being the structure factor (tortuosity). In the high-frequency range, the coefficients g and b must be modified by employing a frequency-correction factor. Here, following Johnson *et al.* (1987), we set

$$b(\omega) = \mathrm{Re}\left(\frac{\eta}{\kappa(\omega)}\right), \qquad g(\omega) = \frac{1}{\omega}\mathrm{Im}\left(\frac{\eta}{\kappa(\omega)}\right), \tag{6}$$

with $\kappa(\omega)$ denoting the dynamic permeability, which is a complex function defined by

$$\kappa(\omega) = \kappa_0\left(\sqrt{1 + \mathrm{i}\frac{4\omega}{n_j\omega_j}} + \mathrm{i}\frac{\omega}{\omega_j}\right)^{-1}. \tag{7}$$

Here κ_0 is the absolute permeability, n_j is a finite parameter determined by the pore geometry (Johnson *et al.* 1987), and ω_j is the viscous-boundary characteristic frequency given by $\omega_j = \eta\phi/(\kappa_0\rho_f S)$.

A plane-wave analysis shows that, in porous fluid-saturated media, there are three types of waves: the Type-I wave that is the analogue of the classical fast P-wave propagating in elastic or viscoelastic isotropic solids, the Type-II

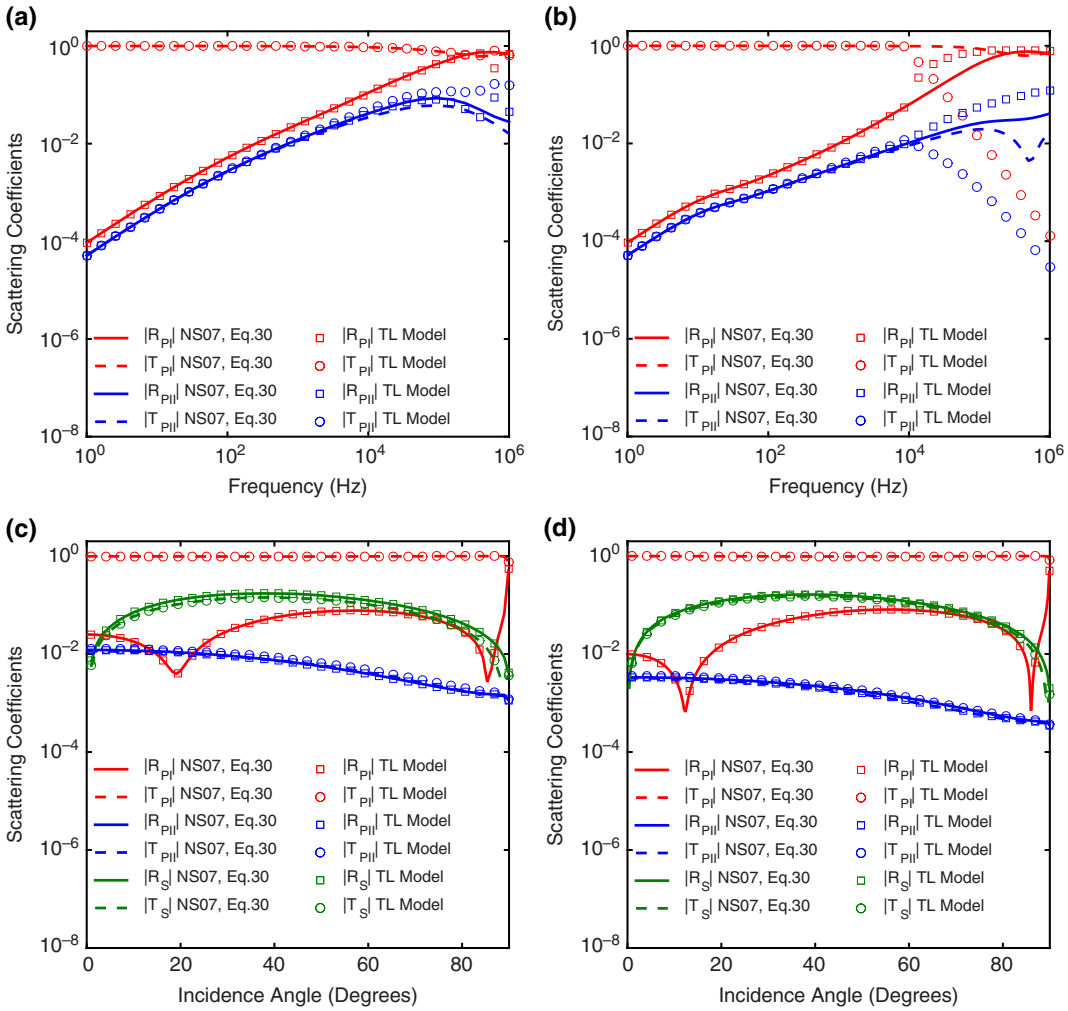

Figure 2 Absolute values of the scattering coefficients for an incident Type I P-wave. The thickness of the fracture is $h = 0.001$ m. The curves labelled *NS07, Eq. 30* correspond to the boundary conditions given by Nakagawa and Schoenberg (2007), whereas the curves labeled *TL model* correspond to the thin layer model. (a) and (b) illustrate normal incidence versus frequency for fracture permeability $\kappa_0 = 100$ D and $\kappa_0 = 0.0001$ D, respectively. At a frequency of 1000 Hz, (c) and (d) show the coefficients versus the incidence angle for fracture permeability $\kappa_0 = 100$ D and $\kappa_0 = 0.0001$ D, respectively.

wave or slow P-wave that correspond to motion out of phase between solid and fluid; and one shear wave (Carcione *et al.* 2010).

3 REFLECTION AND TRANSMISSION COEFFICIENTS OF A SINGLE LAYER

In order to obtain the reflection and transmission (R-T) coefficients of a single layer, we propose to employ a system consisting of three Biot media Ω_n, $n = 1, 2, 3$, with different properties as shown in Fig. 1. Let $z = 0$ be the boundary between Ω_1 and Ω_2, and $z = h$ the boundary between Ω_2 and Ω_3, and consider an incident Type-I compressional plane wave from medium Ω_1 with an angle θ_{iI} with respect to the vertical z-axis. Following Santos *et al.* (2004), we represent the incident, reflected, and transmitted waves using potentials.

For the medium Ω_1, the incident wave potentials of the solid and relative fluid displacements are given by

$$\varphi_{iI} = A_{iI} e^{\mathrm{i}(\omega t - \mathbf{q}_{iI}\cdot\mathbf{x})},$$
$$\psi_{iI} = B_{iI} e^{\mathrm{i}(\omega t - \mathbf{q}_{iI}\cdot\mathbf{x})}, \tag{8}$$

respectively, where $\mathbf{q}_{iI} = q_{iI}(\sin(\theta_{iI}), \cos(\theta_{iI}))$ is the complex wave vector determining the polarization direction, and $\mathbf{x}$ is a distance.

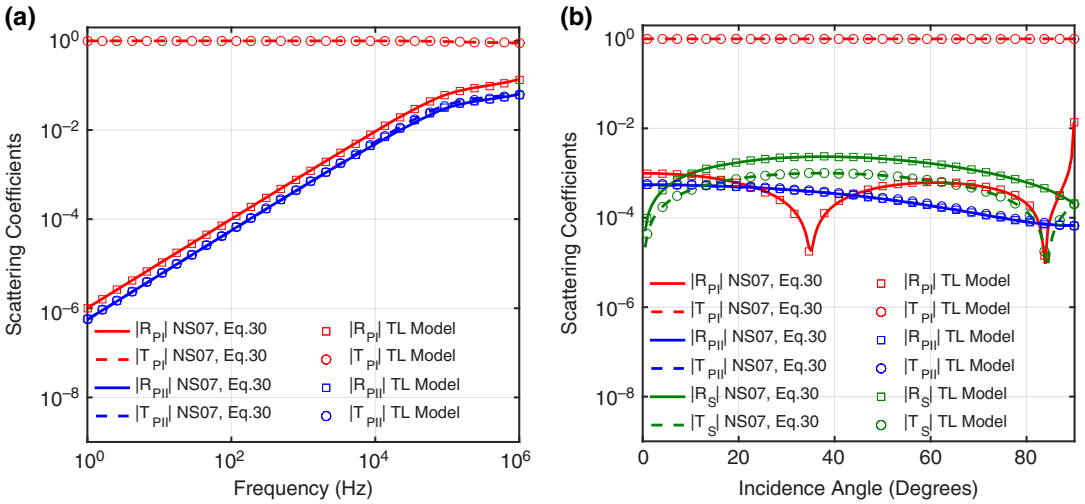

Figure 3 Absolute values of the scattering coefficients for an incident Type I P-wave. The fracture thickness is $h = 0.00001$ m, and the fracture permeability is $\kappa_0 = 0.0001$ D. The labels *NS07, Eq. 30* and *TL model* denote the boundary conditions by Nakagawa and Schoenberg (2007) and by TL model, respectively. (a) shows normal incidence versus frequency, and (b) shows the coefficients versus the incidence angle at frequency = 1,000 Hz.

In Appendix A, we derive from the potentials the amplitude of the R-T coefficients for the different types of waves. This yields the following: expressions:

$$R_j^{(1)} = C_{rj}^{(1)} \frac{q_{rj}^{(1)}}{q_{iI}^{(1)}},$$

$$T_j^{(3)} = C_{tj}^{(3)} \frac{q_{tj}^{(3)}}{q_{iI}^{(1)}}, \quad j = I, II, s. \tag{9}$$

4 SEISMIC BOUNDARY CONDITIONS ACROSS A FRACTURE

The model developed by Nakagawa and Schoenberg (2007) assumes that media Ω_1 and Ω_3 have the same properties, and the thickness of medium Ω_2 tends to zero ($h \to 0$).

In Equation (30) of Nakagawa and Schoenberg (2007), it is assumed that the pressure and fluid velocity within a fracture are given by the superposition of the pressure and fluid velocity at the boundaries with the pressure and fluid velocity for the undrained condition.

Moreover, Nakagawa and Schoenberg (2007) assume that U_x, U_z, σ_{xz}, and σ_{zz} vary linearly, so that the fields vary slowly within the fracture. With these approximations and setting the expressions

$$\widetilde{\rho} = \mathrm{i}\frac{\eta}{\omega\kappa(\omega)},$$

$$\frac{1}{\widetilde{B}} \equiv \alpha^{(2)} + \frac{H_c^{(2)}}{\alpha^{(2)} M^{(2)}} - \left(\frac{\chi}{\omega}\right)^2 \frac{H_c^{(2)}}{\alpha^{(2)}\widetilde{\rho}^{(2)}},$$

$$\widetilde{\beta} \equiv 1 - \frac{H_c^{(2)}\rho_f^{(2)}}{2\alpha^{(2)}\mu^{(2)}\widetilde{\rho}^{(2)}},$$

$$\Pi \equiv \frac{\tanh\epsilon}{\epsilon}, \quad \epsilon \equiv -\frac{\mathrm{i}\beta_{rII}^{(2)} h}{2}; \tag{10}$$

they obtain:

$$\begin{bmatrix} \dot{U}_x^{(3)} - \dot{U}_x^{(1)} \\ \sigma_{zz}^{(3)} - \sigma_{zz}^{(1)} \\ \left(-P_f^{(3)}\right) - \left(-P_f^{(1)}\right) \\ \sigma_{xz}^{(3)} - \sigma_{xz}^{(1)} \\ \dot{U}_z^{(3)} - \dot{U}_z^{(1)} \\ \dot{W}_z^{(3)} - \dot{W}_z^{(1)} \end{bmatrix} = -\frac{\mathrm{i}\omega h}{2} \begin{bmatrix} 0 & \widetilde{\mathrm{Q}}_{XY} \\ \widetilde{\mathrm{Q}}_{YX} & 0 \end{bmatrix} \times \begin{bmatrix} \dot{U}_x^{(3)} + \dot{U}_x^{(1)} \\ \sigma_{zz}^{(3)} + \sigma_{zz}^{(1)} \\ \left(-P_f^{(3)}\right) + \left(-P_f^{(1)}\right) \\ \sigma_{xz}^{(3)} + \sigma_{xz}^{(1)} \\ \dot{U}_z^{(3)} + \dot{U}_z^{(1)} \\ \dot{W}_z^{(3)} + \dot{W}_z^{(1)} \end{bmatrix}, \tag{11}$$

where the dots over the displacement vector components indicate the time derivative. The matrix $\widetilde{\mathrm{Q}}_{XY}$ is given by

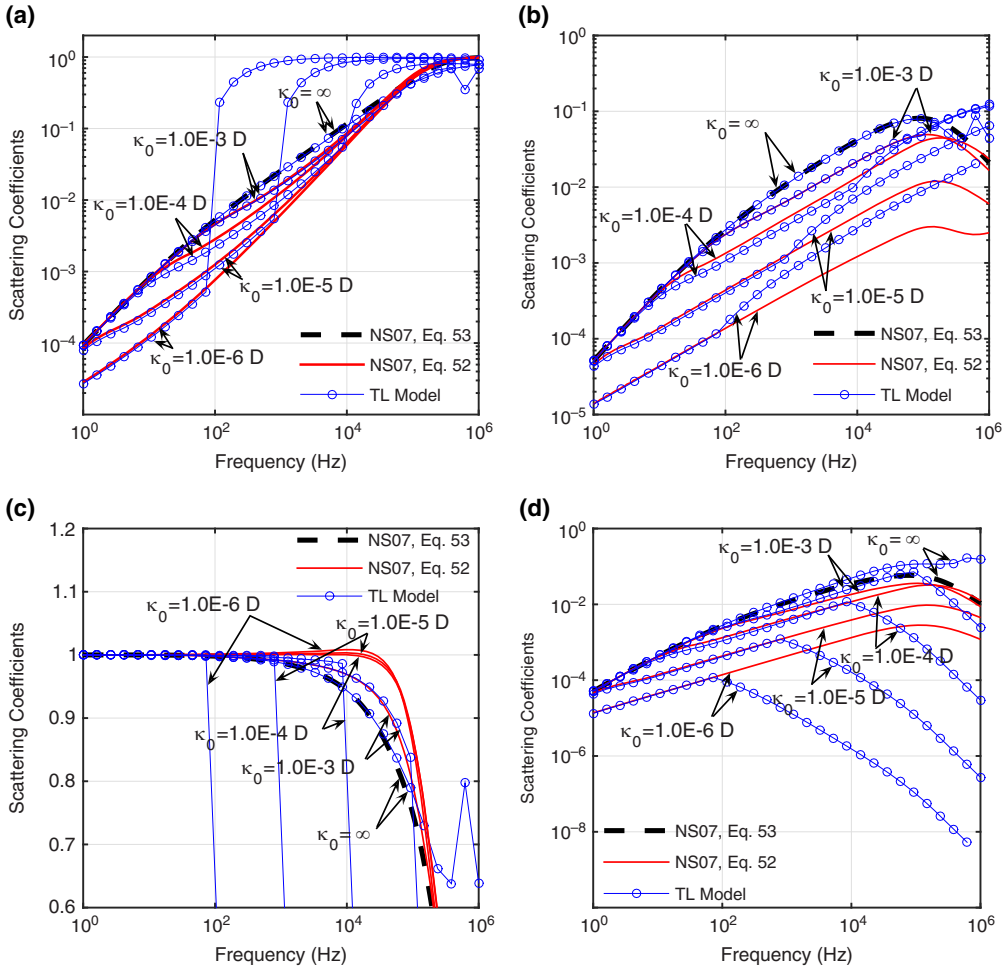

Figure 4 Absolute values of the scattering coefficients of Type I and Type II P-waves as function of frequency. The incident wave is a Type I P-wave, and the fracture features are $h = 0.001$ m, $\phi = 0.5$; the permeability varies from $\kappa_0 = 0.000001$ D to $\kappa_0 =$ infinity. The curves labeled *NS07, Eq. 52* and *NS07, Eq. 53* are for the boundary conditions by Nakagawa and Schoenberg (2007), whereas the curve labelled *TL model* is for the thin layer model. (a) and (b) show the reflection coefficients of Type I and Type II P-waves, respectively. (c) and (d) correspond to the transmission coefficients of Type I and Type II P-waves, respectively.

$$\widetilde{\mathbf{Q}}_{XY} = \begin{bmatrix} 1/\mu^{(2)} & \chi/\omega & 0 \\ \chi/\omega & \rho_b^{(2)} & \rho_f^{(2)} \cdot \Pi \\ 0 & \rho_f^{(2)} & \widetilde{\rho}^{(2)} \cdot \Pi \end{bmatrix}, \tag{12}$$

whereas the elements of the matrix $\widetilde{\mathbf{Q}}_{YX}$ are given in Appendix B.

Let us characterize the properties of the fracture through the following parameters also proposed by Nakagawa and Schoenberg (2007):

- Shear compliance $\eta_T = \frac{h}{\mu^{(2)}}$;
- Dry or drained normal compliance $\eta_{N_D} = \frac{h}{H_c^{(2)}}$;
- Membrane permeability $\widehat{\kappa}(\omega) = \frac{\kappa^{(2)}(\omega)}{h}$.

Then, multiplying $\widetilde{\mathbf{Q}}_{XY}$ and $\widetilde{\mathbf{Q}}_{YX}$ by h and eliminating the $O(h)$-terms, since $\widetilde{\beta} \approx 1$, (11) reduces to

$$\begin{cases} \dot{U}_x^{(3)} - \dot{U}_x^{(1)} = (-\mathrm{i}\omega)\,\eta_T \sigma_{xz}^{(1)} \\ \dot{U}_z^{(3)} - \dot{U}_z^{(1)} = (-\mathrm{i}\omega)\,\eta_{N_D}\left[\left(1-\alpha^{(2)}\widetilde{B}\,(1-\Pi)\right)\sigma_{zz}^{(1)} \right. \\ \qquad\qquad \left. - \alpha^{(2)}\frac{-P_f^{(3)}+\left(-P_f^{(1)}\right)}{2}\cdot\Pi\right] \\ \dot{W}_z^{(3)} - \dot{W}_z^{(1)} = (-\mathrm{i}\omega)\,\alpha^{(2)}\eta_{N_D} \\ \qquad\qquad \times\left[-\sigma_{zz}^{(1)} + \frac{1}{B}\frac{-P_f^{(3)}+\left(-P_f^{(1)}\right)}{2}\right]\cdot\Pi \\ \sigma_{xz}^{(3)} = \sigma_{xz}^{(1)} \\ \sigma_{zz}^{(3)} = \sigma_{zz}^{(1)} \\ -P_f^{(3)} - \left(-P_f^{(1)}\right) = \frac{\eta_f^{(2)}}{\widehat{\kappa}(\omega)}\frac{\dot{W}_z^{(3)}+\dot{W}_z^{(1)}}{2}\cdot\Pi \end{cases} \tag{13}$$

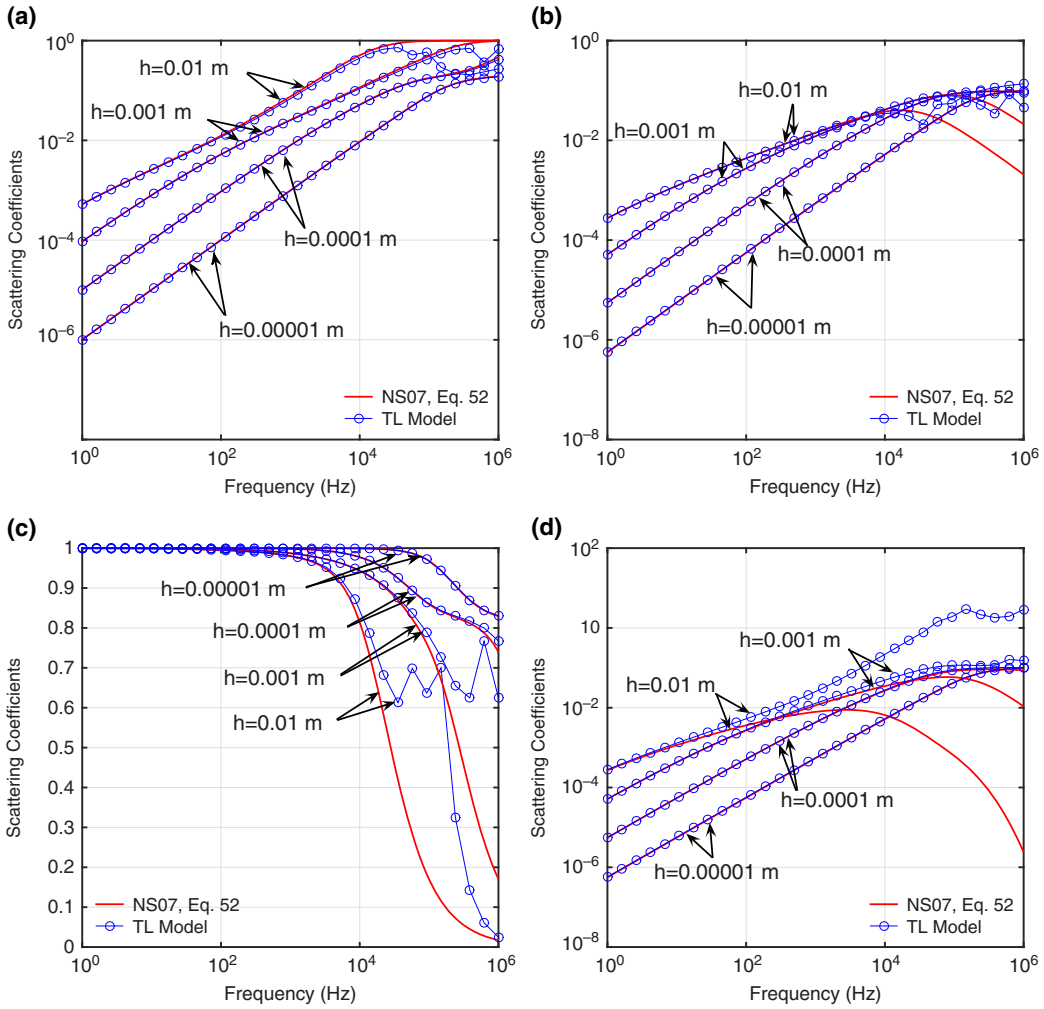

Figure 5 Absolute values of the scattering coefficients of Type I and Type II P-waves versus frequency. The incident wave is a Type I P-wave, and the fracture features are $\kappa_0 = 1.0$ D and $\phi = 0.5$; the thickness h varies from 0.00001 m to 0.01 m. The label *NS07, Eq. 52* refers to the boundary conditions by Nakagawa and Schoenberg (2007). The label *TL model* refers to the thin layer model. (a) and (b) illustrate the reflection coefficients of Type I and Type II P-waves, respectively. (c) and (d) correspond to the transmission coefficients of Type I and Type II P-waves, respectively.

where

$$\widetilde{B} = \alpha^{(2)} \frac{M^{(2)}}{H_u^{(2)}},$$

$$H_u^{(2)} = K_u^{(2)} + \frac{4\mu^{(2)}}{3},$$

$$\epsilon = \frac{1-i}{2}\sqrt{\omega \frac{\alpha^{(2)}\eta_f \eta_{N_D}}{2\widetilde{B}\widehat{\kappa}_0}}, \quad \widehat{\kappa}_0 = \kappa_0 / h. \tag{14}$$

Equation (13) is equation (52) of Nakagawa and Schoenberg (2007).

Finally, when the permeability tends to infinity in equation (13), we get equation (53) of Nakagawa and Schoenberg (2007):

$$\begin{cases} \dot{U}_x^{(3)} - \dot{U}_x^{(1)} = (-\mathrm{i}\omega)\,\eta_T \sigma_{xz}^{(1)} \\ \dot{U}_z^{(3)} - \dot{U}_z^{(1)} = (-\mathrm{i}\omega)\,\eta_{N_D}\left[\sigma_{zz}^{(1)} - \alpha^{(2)}\left(-P_f^{(1)}\right)\right] \\ \dot{W}_z^{(3)} - \dot{W}_z^{(1)} = (-\mathrm{i}\omega)\,\alpha^{(2)}\eta_{N_D}\left[-\sigma_{zz}^{(1)} + \frac{1}{B}\left(-P_f^{(1)}\right)\right] \\ \sigma_{xz}^{(3)} = \sigma_{xz}^{(1)} \\ \sigma_{zz}^{(3)} = \sigma_{zz}^{(1)} \\ -P_f^{(3)} = -P_f^{(1)}. \end{cases} \tag{15}$$

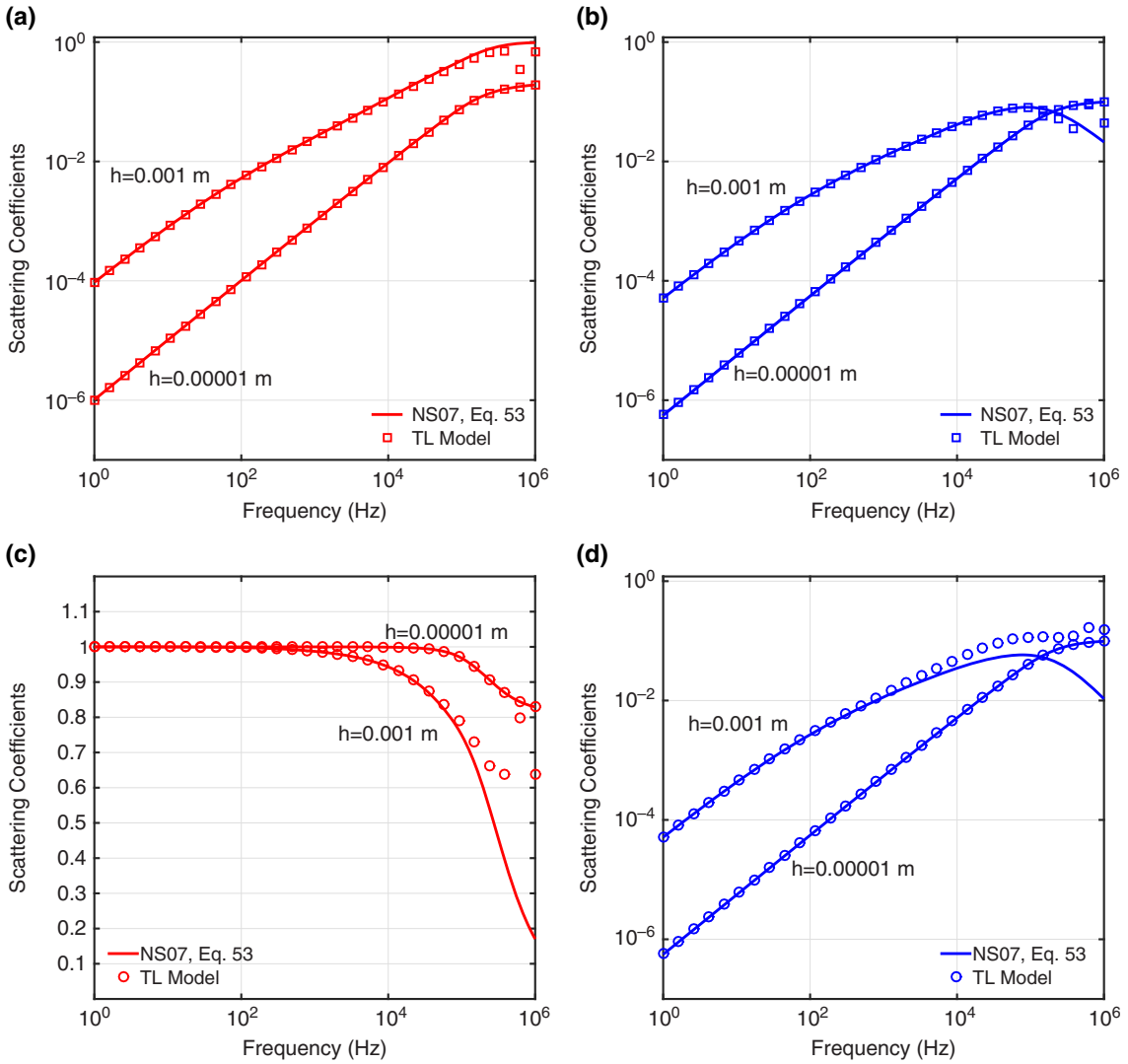

Figure 6 Absolute values of the scattering coefficients of Type I and Type II P-waves versus frequency for an incident Type I P-wave. The porosity is 0.5, and the permeability $\kappa_0 \to \infty$. The fracture thickness h is indicated in the different curves. The curve labeled *NS07, Eq. 53* corresponds to the boundary conditions by Nakagawa and Schoenberg (2007), whereas the curve labelled *TL model* corresponds to the thin layer model. (a) and (b) show the reflection coefficients of Type I and Type II P-waves, respectively. (c) and (d) illustrate the transmission coefficients of Type I and Type II P-waves, respectively.

These boundary conditions mean a balance of the fluid pressure on both sides of the fracture, and the fluid is allowed to move freely. Then, these concepts of open fracture are manifested in equations (15).

The calculation of the relection and transmission (R-T) coefficients associated with the boundary conditions in (11), (13), and (15) was done by employing potentials as explained in Appendix A for the case of the fracture represented as a thin layer. In this way, the system of equations, similar to that in (A27), is shown in (B2), and its matrix form becomes

$$(\mathbf{N}\cdot\mathbf{D})\mathbf{r} = \mathbf{i}'_p, \quad \text{where} \quad \mathbf{N} = N_{i,j},$$
$$\mathbf{D} = \text{diag}\left[1, 1, 1, e^{-i\beta^{(3)}_{t1}h}, e^{-i\beta^{(3)}_{t11}h}, e^{-i\beta^{(3)}_{ts}h}\right]. \tag{16}$$

After solving equation (16) for **r**, the R-T coefficients are computed using (9).

5 EXAMPLES

In this section, we compare the R–T coefficients at a fracture represented either using the boundary conditions (11), (13) and (15) or a thin layer (TL model). In the TL model,

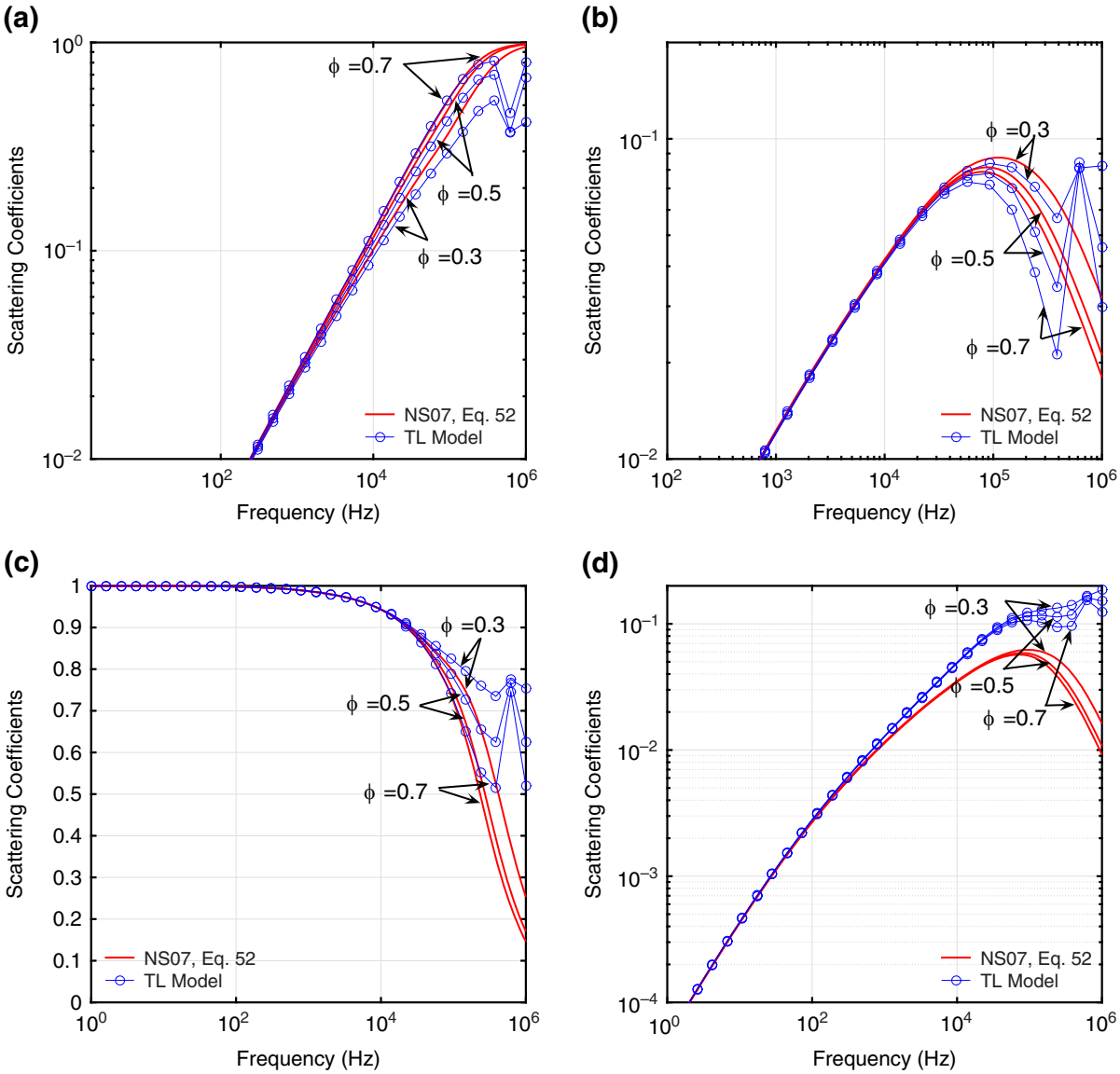

Figure 7 Absolute values of the scattering coefficients of Type I and Type II P-waves versus frequency for an incident Type I P-wave. The fracture properties are $\kappa_0 = 1.0$ D and $h = 0.001$ m, and values of ϕ are shown in the different curves. The curve labeled *NS07, Eq. 52* refers to the boundary conditions by Nakagawa and Schoenberg (2007). The curve labeled *TL model* refers to the thin layer model. (a) and (b) display the reflection coefficients of Type I and Type II P-waves, respectively. (c) and (d) illustrate the transmission coefficients of Type I and Type II P-waves, respectively.

the R-T coefficients are given by equation (A26) assuming h much smaller than the signal wavelength. Let us define the fracture-thickness/wavelength ratio $\mathcal{R}$, where the wavelength is that of the Type I-wave of the background medium. We consider several cases of interest in reservoir geophysics. The background and fracture properties are indicated in Table 1 and fluid properties are shown in Table 2. The following cases are taken into account.

Case 1: Comparison between the TL model and the boundary condition (11) (equation (30) of Nakagawa and Schoenberg (2007)).

Case 2: Comparison between the TL model and the boundary conditions (13) and (15) (equations (52) and (53) of Nakagawa and Schoenberg (2007)).

Case 3: Calculation of the R-T coefficients at a fracture represented with the boundary condition (13), with water in

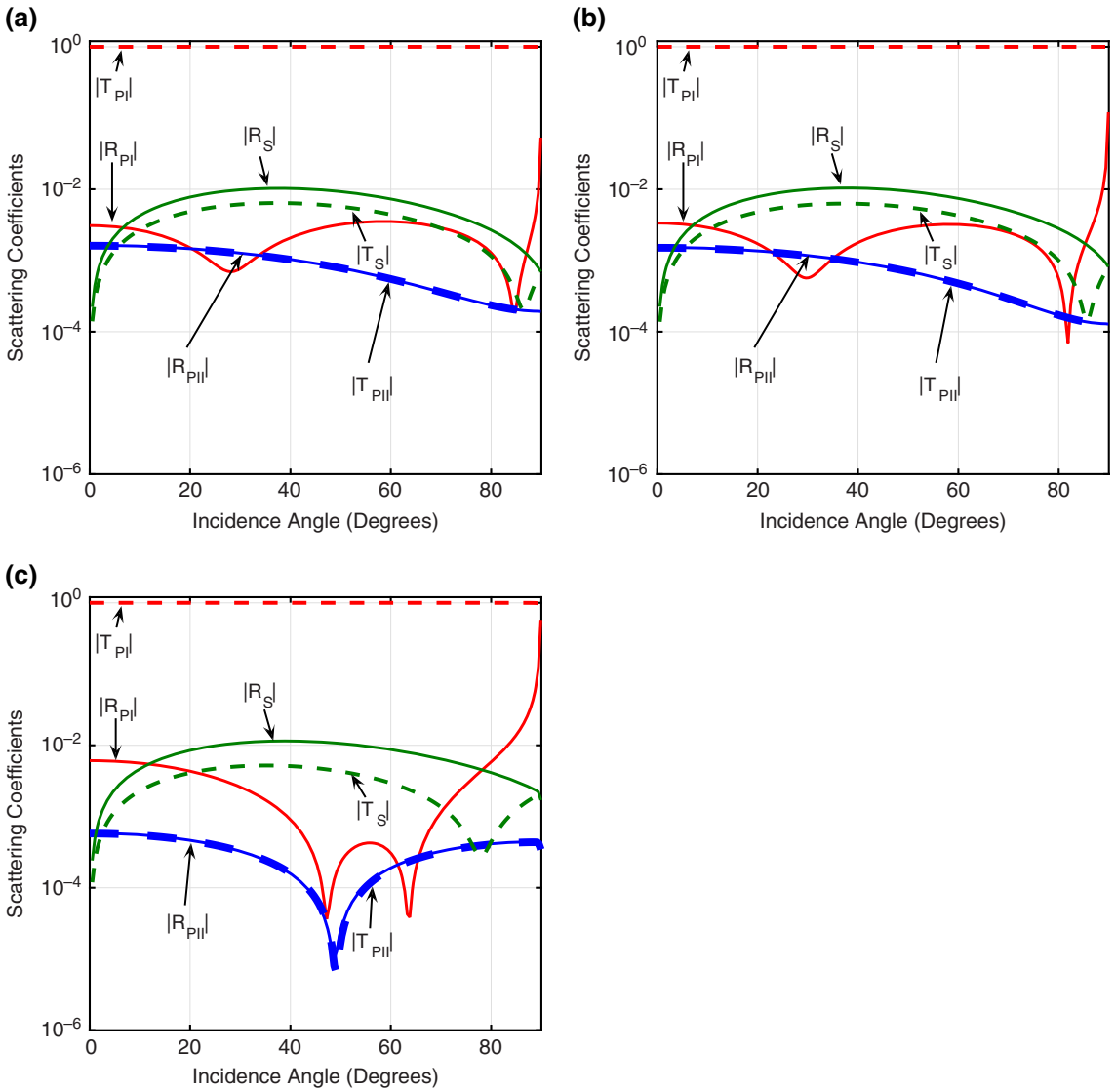

Figure 8 Scattering coefficients (absolute values of the R-T coefficients) of Type I, Type II, and shear waves as a function of the incidence angle. Background is water saturated. The coefficients are calculated using (13). The incident wave is a Type I P-wave of frequency 50 Hz, permeability κ_0 is 100 D, fracture thickness h is 0.001 m. (a) Water in the fracture, (b) oil in the fracture, and (c) gas in the fracture.

the background medium and three different fluids saturating the fracture.

5.1 Case 1

We compute the R-T coefficients for compressional plane waves propagating through a fracture, with the three media being saturated for water. We choose two values of permeability for the fracture: one very low ($\kappa_0 = 0.0001$ D) and the other very high ($\kappa_0 = 100$ D) to analyse their influence on the R-T coefficients.

Figure 2 shows the magnitude of the scattering coefficients (R-T coefficients) for the TL model and equation (30) of Nakagawa and Schoenberg (2007). The R-T coefficients are given as function of frequency at normal incidence and a function of the the incidence angle at 1000 Hz, so that $\mathcal{R} = 3.1 \times 10^{-4}$ (fracture aperture $h = 0.001$ m and wavelength $\lambda = 3.2$ m). It can be seen noticeable differences between the two models for the case of very low permeability, when the permeability of the fracture is less than the permeability of the background (Fig. 2 b, d).

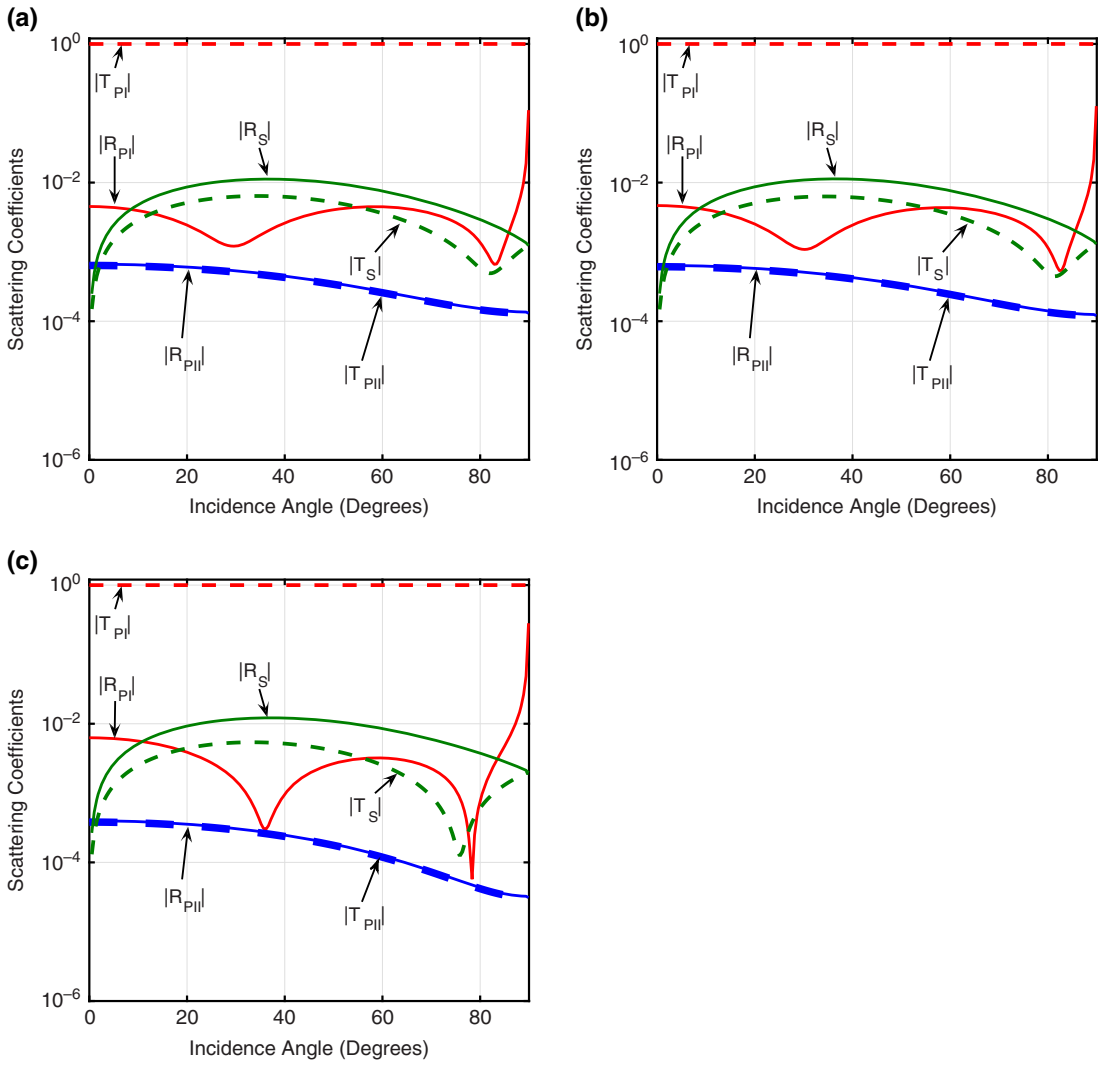

Figure 9 Scattering coefficients (absolute values of the R-T coefficients) of Type I, Type II, and shear waves as a function of the incidence angle. Background is oil saturated. The coefficients are calculated using (13). The incident wave is a Type I P-wave of frequency 50 Hz, permeability κ_0 is 100 D, fracture thickness h is 0.001 m. (a) Water in the fracture, (b) oil in the fracture, and (c) gas in the fracture.

Figure 3 shows the same R-T coefficients with that in Fig. 2 but for a smaller fracture aperture ($h = 0.00001$ m), $\kappa_0 = 0.0001$ D, and a frequency of 1000 Hz, so that $\mathcal{R} = 3.1 \times 10^{-6}$. Here, the coefficients obtained with the two models coincide.

5.2 Case 2

In this case, the TL model is compared with (13) and (15). Three tests were performed, varying the permeability, porosity, and fracture aperture while the background and the fracture are saturated with water.

1. Varying permeability :

The incident wave is a Type I P-wave, the fracture thickness is h= 0.001 m, its porosity $\phi = 0.5$, and the other parameters are as shown in Table 1; the fracture permeability varies from 0.000001 D and infinite. Figure 4, shows the reflection and transmission coefficients, for five different permeability values.

It is observed that, for high values of permeability, the R-T coefficients of the TL Model and those associated with the three boundary conditions analyzed are similar. Equation (15), fits very well with the thin layer model, except for very high frequencies (above 1×10^{5} Hz).

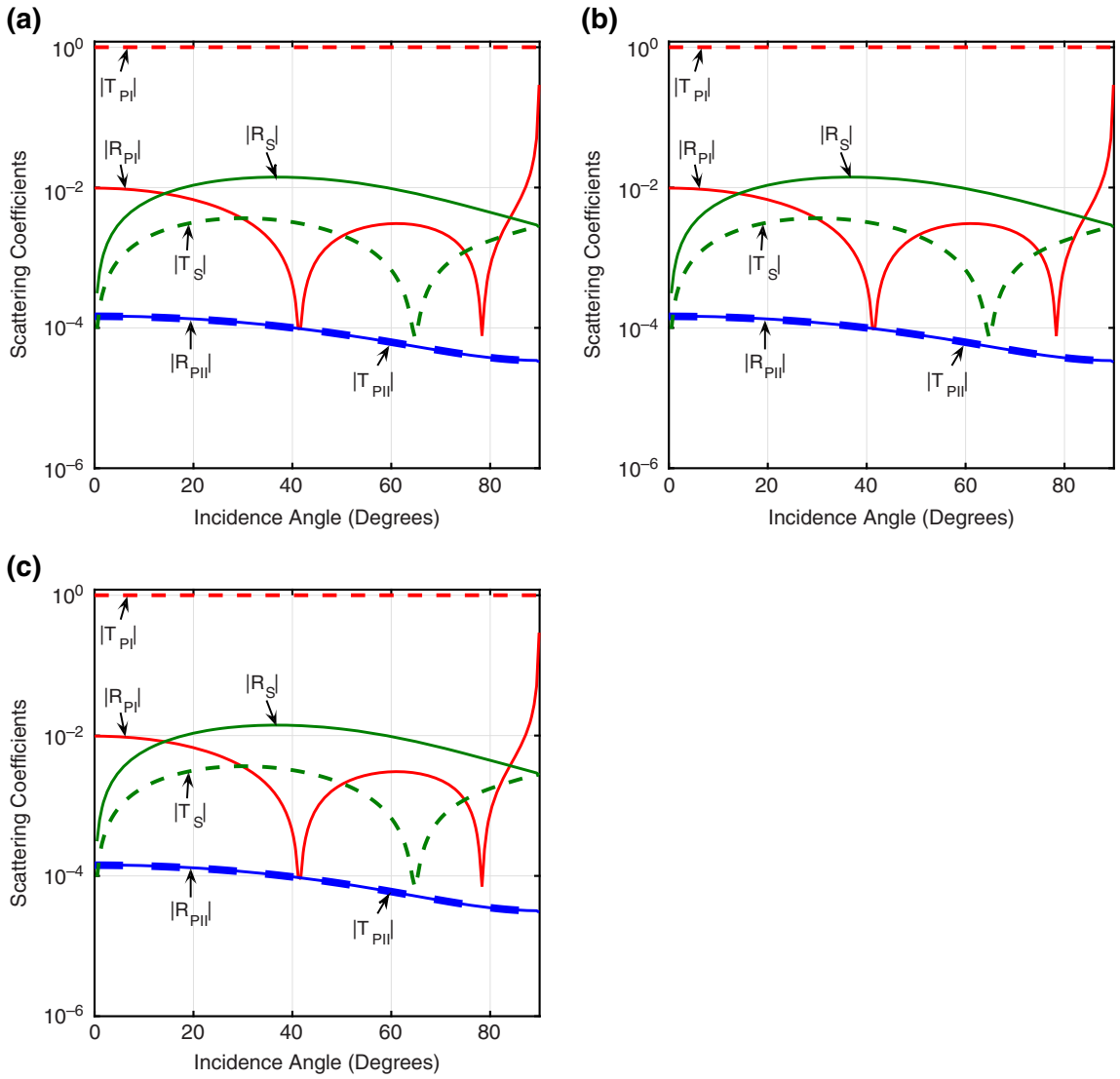

Figure 10 Scattering coefficients (absolute values of the R-T coefficients) of Type I, Type II, and shear waves as a function of the incidence angle. Background is gas saturated. The coefficients are calculated using (13). The incident wave is a Type I P-wave of frequency 50 Hz, permeability κ_0 is 100 D, fracture thickness h is 0.001 m. (a) Water in the fracture, (b) oil in the fracture, and (c) gas in the fracture.

When the permeability of the fracture is much higher that the permeability of background (in this case, the background permeability is 0.1 D), there is a good fit between the model of the thin layer and the boundary conditions, for most values of frequency.

2. Variation in the fracture thickness:

The incident wave is a Type I P-wave, but now, permeability is $\kappa_0 = 1.0$ D, porosity $\phi = 0.5$, and we vary the the fracture thickness. In Figs. 5 and 6, it is shown that the best fit among the TL model and the three boundary conditions occurs when the value of h decreases. As expected, if the fracture is very thin, the reflection coefficients become smaller.

Close to 100 Hz, there is a good fit between the thin layer and the boundary conditions, for all values of h. At this frequency, the wavelength is $\lambda = 32.02$ m and for $h = 0.01$ m, 0.001 m, 0.0001 m, and 0.00001 m, the corresponding values of $\mathcal{R}$ are 3.1×10^{-4}, 3.1×10^{-5}, 3.1×10^{-6}, and 3.1×10^{-7}, respectively.

3. Varying porosity

Finally the reflection and transmission coefficients are calculated by varying the porosity of the fracture, i.e., $\phi = 0.3$, 0.5,

and 0.7. The incident wave is a Type I P-wave, $h = 0.001$ m, and $\kappa_0 = 1.0$ D. Figure 7 shows the results, where a good fit is observed at low frequencies for all porosity values.

5.3 Case 3

Here we compute the R-T coefficients using the boundary condition (13) as function of the incidence angle at a frequency of 50 Hz and for three different cases of interest in reservoir geophysics. The parameters of the background and fracture are shown in Tables 1 and 2. In all cases, the frequency is 50 Hz, the fracture permeability κ_0 is 100 D, the fracture porosity ϕ is 0.5, and the fracture thickness h is 0.001 m.

- Water in background:
  The background Biot medium is saturated with water so that $\mathcal{R} = 1.6 \times 10^{-5}$ (wavelength $\lambda = 64.06$ m), and the fracture contains water, oil, or gas. Figure 8 displays the R-T coefficients. It can be seen that although, for water and oil saturating the fracture (Fig. 8a,b), the R-T coefficients show a similar behavior, the R-T coefficients for the gas-saturated case (Fig. 8c) display completely different patterns. In Fig. 8(c) we observe peaks at 46° and 64° for the reflection coefficient of the Type I wave, and a peak at 50° for the R-T coefficient of the Type II P-wave, probably indicating phase changes, as was observed by Martinez *et al.* (2014). The peaks of the reflection coefficient of the Type I wave are already present in the water and oil saturated cases, but farther apart and much smoother than in the gas case.
- Oil in background:
  Here the background medium is oil saturated, so that $\mathcal{R} = 1.7 \times 10^{-5}$ (wavelength $\lambda = 58.22$ m), whereas the fracture is saturated with water, oil, or gas. Figure 9 shows R-T coefficients, showing close similarities for water and oil in the fracture (Fig. 9a, b). Instead, when gas fills the fracture, the R-T coefficients are quite different of those in the water or oil cases, with the stronger differences observed for the reflection coefficient of Type I-waves and the transmission coefficient of shear waves.
- Gas in background:
  Finally the background is gas-saturated with $\mathcal{R} = 1.76 \times 10^{-5}$ (wavelength $\lambda = 56.59$ m) and the fracture is again saturated with water, oil, or gas. Figure 10 shows the R-T coefficients for the three fluids saturating the fracture, with no observable differences in the R-T coefficients.

6 CONCLUSIONS

In all cases analysed, at seismic frequencies, we observed a very good fit of the reflection and transmission coefficients for all forms of the Nakagawa and Schoenberg (2007) boundary conditions when compared with the thin-layer model. In numerical simulations, these results allow us to consider boundary conditions to represent fractures, avoiding the use of extremely fine computational meshes required to model thin layers.

When the background Biot medium is water saturated and the fracture is saturated with water or oil, little differences can be observed in the R-T coefficients. Instead, when the fracture is gas saturated, the Type I reflection coefficient shows a different behavior to the water or oil cases, with peaks at 46° and 64°. The Type II wave R-T coefficients also behave differently than in the water and oil cases, with a peak close to 50°, indicating that fractures may play an important role in the mesoscopic loss mechanism.

When the background is oil saturated and the fracture is saturated by water, oil, or gas, the R-T coefficients show in general the same patterns than for the water-saturated background case, although in the gas case, the peaks of the the Type I reflection coefficient are located at 35° and 80°.

If the background is gas saturated, the R-T coefficients show a very similar behaviour independently of the type of fluid saturating the fractures.

This quite different acoustic fracture response for different fluids filling a fracture may be used to infer the distinct fluid type saturating the fractures.

ACKNOWLEDGEMENTS

This work was supported in part by the Agencia Nacional de Promoción Científica y Tecnológica, Argentina through FONARSEC FSTIC 06/10 and by CONICET from PIP 0952. The work of J. M. Carcione was supported in part by the CO2Monitor project.

REFERENCES

Bakke N.E. and Ursin B. 1998. Thin-bed AVO effects. *Geophysical Prospecting* **46**, 571–587.

Bakulin A.V. and Molotkov L.A. 1997. Poroelastic medium whit fractures at limiting case of stratified poroelastic medium with thin and soft Biot layers. 67th SEG meeting, Madrid, Spain, Expanded Abstracts, 1001–1004.

Berryman J.G. 1980. Confirmation of Biot's theory. *Applied Physics Letters* **37**, 382–384.

Berryman J.G. 1982. Elastic waves in fluid-saturated porous media. In: *Macroscopic Properties of Disordered Media*, pp. 38–50. Springer-Verlag Berlin Heidelberg.

Biot M.A. 1956. Theory of propagation of elastic waves in a fluid-saturated porous solid. I. Low-frequency range. *The Journal of the Acoustical Society of America* **28**, 168–178.

Biot M.A. 1962. Mechanics of deformation and acoustic propagation in porous media. *Journal of Applied Physics* **33**, 1482–1498.

Brekhovskikh L.M. 1980. *Waves in Layered Media, 2nd edn*., pp. 503. Academic Press Inc., New York.

Carcione J.M. 1996. Elastodynamics of a non-ideal interface: application to crack and fracture scattering. *Journal of Geophysical Research: Solid Earth* **101**, 28177–28188.

Carcione J.M. 1997. Reflection and transmission of qP–qS plane waves at a plane boundary between viscoelastic transversely isotropic media. *Geophysical Journal International* **129**, 669–680.

Carcione J.M. 1998. Scattering of elastic waves by a plane crack of finite width in a transversely isotropic medium. *International Journal for Numerical and Analytical Methods in Geomechanics* **22**, 263–275.

Carcione J.M. 2001. Amplitude variations with offset of pressure-seal reflections. *Geophysics* **66**, 283–293.

Carcione J.M. 2015. *Wave Fields in Real Media: Wave Propagation in Anisotropic, Anelastic, Porous and Electromagnetic Media, 3rd edn*. Elsevier, Amsterdam.

Carcione J.M., Gurevich B. and Cavallini F. 2000. A generalized Biot–Gassmann model for the acoustic properties of shaley sandstones. *Geophysical Prospecting* **48**, 539–557.

Carcione J.M., Morency C. and Santos J.E. 2010. Computational poroelasticity-A review. *Geophysics* **75**, A229–A243.

Carcione J.M. and Picotti S. 2012. Reflection and transmission coefficients of a fracture in transversely isotropic media. *Studia Geophysica et Geodaetica* **56**, 307–322.

Carcione J.M., Santos J.E., Ravazzoli C.L. and Helle H.B. 2003. Wave simulation in partially frozen porous media with fractal freezing conditions. *Journal of Applied Physics* **94**, 7839–7847.

Chung H.M. and Lawton D.C. 1995. Amplitude responses of thin beds: Sinusoidal approximation versus Ricker approximation. *Geophysics* **60**, 223–230.

Chung H.M. and Lawton D.C. 1996. Frequency characteristics of seismic reflections from thin beds. *Canadian Journal of Exploration Geophysics* **31**, 32–37.

Daley T.M. 2006. Fractured reservoirs: an analysis of coupled elastodynamic and permeability changes from pore-pressure variation. *Geophysics* **71**(5), O33.

Dutta N.C. and Odé H. 1979a. Attenuation and dispersion of compressional waves in fluid-filled porous rocks with partial gas saturation (White model)—Part I: Biot theory. *Geophysics* **44**, 1777–1788.

Dutta N.C. and Odé H. 1979b. Attenuation and dispersion of compressional waves in fluid-filled porous rocks with partial gas saturation (White model)—Part II: Results. *Geophysics* **44**, 1789–1805.

Dutta N.C. and Odé H. 1983. Seismic reflections from a gas-water contact. *Geophysics* **48**, 14–32.

Fellah M., Fellah Z.E.A., Mitri F.G., Ogam E. and Depollier C. 2013. Transient ultrasound propagation in porous media using Biot theory and fractional calculus: Application to human cancellous bone. *The Journal of the Acoustical Society of America* **133**, 1867–1881.

Gu B.L., Nihei K.T., Myer L.R. and Pyrak-Nolte L.J. 1996. Fracture interface waves. *Journal of Geophysical Research: Solid Earth* **101**, 827–835.

Hsu C.J. and Schoenberg M. 1993. Elastic waves through a simulated fractured medium. *Geophysics* **58**, 964–977.

Jocker J. and Smeulders D. 2009. Ultrasonic measurement on poroelastic slabs: Determination of reflection and transmission coefficients and processing for Biot input parameters. *Ultrasonics* **49**, 319–330.

Johnson D.L., Koplik J. and Dashen R. 1987. Theory of dynamic permeability and tortuosity in fluid-saturated porous media. *Journal of Fluid Mechanics* **176**, 379–402.

Johnson D.L., Plona T.J. and Kojima H. 1994. Probing porous media with first and second sound II. Acoustic properties of water saturated porous media. *Journal of Applied Physics* **76**, 115–125.

Juhlin C. and Young R. 1993. Implication of thin layers for amplitude variation with offset (AVO) studies. *Geophysics* **58**, 1200–1204.

Kong L., Gurevich B., Muller T.M., Wang Y. and Yang H. 2013. Effect of fracture fill on seismic attenuation and dispersion in fractured porous rocks. *Geophysical Journal International* **195**(3), 1679–1688.

Krief M., Garat J., Stellingwerff J. and Ventre J. 1990. A petrophysical interpretation using the velocities of P and S waves (full waveform sonic). *The Log Analyst* **31**, 355–369.

Lambert G., Gurevich B. and Brajanovski M. 2005. Frequncy-dependent anisotropy of porous rocks with aligned fractures. In: *Proceedings of the Poromechanics III - Biot Centennial (1905-2005)*, pp. 309–314.

Liu L. and Schmitt D.R. 2003. Amplitude and AVO responses of a single thin bed. *Geophysics* **68**, 1161–1168.

Martinez C.R., Santos J., Gauzellino P. M. and Carcione J.M. 2014. Reflection and transmission coefficients of a single layer in poroelastic media. *The Journal of the Acoustical Society of America* **135**, 3151–3162.

Molotkov L.A. 2004. Wave propagation in anelastic medium intersected by systems of parallel fractures. *Journal of Mathematical Sciences* **122**, 3548–3563.

Molotkov L.A. and Bakulin A.V. 1997. An effective model of a fractured medium with fractures modeled by the surfaces of discontinuity of displacements. *Journal of Mathematical Sciences* **86**, 2735–2751.

Nakagawa S. and Schoenberg M.A. 2007. Poroelastic modeling of seismic boundary conditions across a fracture. *The Journal of the Acoustical Society of America* **122**, 831–847.

Pilant W.L. 1979. *Elastic Waves in the Earth*. Elsevier Science Publishing Company, Amsterdam.

Plona T. 1980. Observation of a second bulk compressional wave in a porous medium at ultrasonic frequencies. *Applied Physics Letters* **36**, 259–261.

Pride S.R., Tromeur E. and Berryman J.G. 2002. Biot slow-wave effects in stratified rock. *Geophysics* **67**, 271–281.

Pyrak-Nolte L., Cook N.G.W. and Myer L.R. 1990. Transmission of seismic waves across single natural fractures. *Journal of Geophysical Research* **95**, 8516–8538.

Quintal B., Schmalholz S.M. and Podladchikov Y. Y. 2009. Low-frequency reflections from a thin layer with high attenuation caused by interlayer flow. *Geophysics* **74**, N14–N22.

Rubino J.G., Ravazzoli C.L. and Santos J.E. 2006. Reflection and transmission of waves in composite porous media: A quantification of energy conversions involving slow waves. *The Journal of the Acoustical Society of America* **120**, 2425–2436.

Santos J.E., Corbero J.M., Ravazzoli C.L., and Hensley J.L. 1992. Reflection and transmission coefficients in fluid-saturated porous media. *The Journal of the Acoustical Society of America* **91**, 1911–1923.

Santos J.E., Ravazzoli C.L., and Carcione J.M. 2004. A model for wave propagation in a composite solid matrix saturated by a single-phase fluid. *The Journal of the Acoustical Society of America* **115**, 2749–2760.

Schmidt H. and Tango G. 1986. Efficient global matrix approach to the computation of synthetic seismograms. *Geophysical Journal of the Royal Astronomical Society* **84**, 331–359.

Schoenberg M. 1980. Elastic wave behavior across linear slip interfaces. *The Journal of the Acoustic Society of America* **68**, 1516–1521.

Widess M.B. 1973. How Thin is a Thin Bed? *Geophysics* **38**, 1176–1180.

Wu K., Xue Q. and Adler L. 1990. Reflection and transmission of elastic waves from a fluid-saturated porous solid boundary. *The Journal of the Acoustical Society of America* **87**, 2346–2358.

APPENDIX A: THIN-LAYER MODEL

In this appendix, following Martinez *et al.* (2014), we explain how to compute the R–T coefficients for the case of the fracture represented as a thin layer (TL model). Reflected and transmitted waves are represented as potentials, similarly to the incident wave in (8).

Let $\varphi_{rc}^{(1)}$ and $\varphi_{rs}^{(1)}$ be the compressional potentials of the solid, and let $\psi_{rc}^{(1)}$ and $\psi_{rs}^{(1)}$ be shear potentials of the relative fluid displacements, for the reflected waves in Ω_1. They are given by

$$\begin{aligned}
\varphi_{rc}^{(1)} &= A_{rI}^{(1)} e^{i(\omega t - \mathbf{q}_{rI}^{(1)}\cdot\mathbf{x})} + A_{rII}^{(1)} e^{i(\omega t - \mathbf{q}_{rII}^{(1)}\cdot\mathbf{x})},\\
\varphi_{rs}^{(1)} &= A_{rs}^{(1)} e^{i(\omega t - \mathbf{q}_{rs}^{(1)}\cdot\mathbf{x})},\\
\psi_{rc}^{(1)} &= B_{rI}^{(1)} e^{i(\omega t - \mathbf{q}_{rI}^{(1)}\cdot\mathbf{x})} + B_{rII}^{(1)} e^{i(\omega t - \mathbf{q}_{rII}^{(1)}\cdot\mathbf{x})},\\
\psi_{rs}^{(1)} &= B_{rs}^{(1)} e^{i(\omega t - \mathbf{q}_{rs}^{(1)}\cdot\mathbf{x})},
\end{aligned} \tag{A1}$$

where the subscript r indicates the reflected wave for the compressional and shear waves (subscripts c and s). The superscript (1) refers to medium Ω_1 and subscripts I and II indicate Type-I and Type-II waves, respectively.

The potentials in the medium Ω_2 are denoted by

$$\begin{aligned}
\varphi_{tc}^{(2)} &= A_{tI}^{(2)} e^{i(\omega t - \mathbf{q}_{tI}^{(2)}\cdot\mathbf{x})} + A_{tII}^{(2)} e^{i(\omega t - \mathbf{q}_{tII}^{(2)}\cdot\mathbf{x})},\\
\varphi_{ts}^{(2)} &= A_{ts}^{(2)} e^{i(\omega t - \mathbf{q}_{ts}^{(2)}\cdot\mathbf{x})},\\
\psi_{tc}^{(2)} &= B_{tI}^{(2)} e^{i(\omega t - \mathbf{q}_{tI}^{(2)}\cdot\mathbf{x})} + B_{tII}^{(2)} e^{i(\omega t - \mathbf{q}_{tII}^{(2)}\cdot\mathbf{x})},\\
\psi_{ts}^{(2)} &= B_{ts}^{(2)} e^{i(\omega t - \mathbf{q}_{ts}^{(2)}\cdot\mathbf{x})},\\
\varphi_{rc}^{(2)} &= A_{rI}^{(2)} e^{i(\omega t - \mathbf{q}_{rI}^{(2)}\cdot\mathbf{x})} + A_{rII}^{(2)} e^{i(\omega t - \mathbf{q}_{rII}^{(2)}\cdot\mathbf{x})},\\
\varphi_{rs}^{(2)} &= A_{rs}^{(2)} e^{i(\omega t - \mathbf{q}_{rs}^{(2)}\cdot\mathbf{x})},\\
\psi_{rc}^{(2)} &= B_{rI}^{(2)} e^{i(\omega t - \mathbf{q}_{rI}^{(2)}\cdot\mathbf{x})} + B_{rII}^{(2)} e^{i(\omega t - \mathbf{q}_{rII}^{(2)}\cdot\mathbf{x})},\\
\psi_{rs}^{(2)} &= B_{rs}^{(2)} e^{i(\omega t - \mathbf{q}_{rs}^{(2)}\cdot\mathbf{x})}
\end{aligned} \tag{A2}$$

where the subscript t indicates the transmitted wave, and the superscript (2) refers the medium Ω_2.

Finally, the potentials in the medium Ω_3 are,

$$\begin{aligned}
\varphi_{tc}^{(3)} &= A_{tI}^{(3)} e^{i(\omega t - \mathbf{q}_{tI}^{(3)}\cdot\mathbf{x})} + A_{tII}^{(3)} e^{i(\omega t - \mathbf{q}_{tII}^{(3)}\cdot\mathbf{x})},\\
\varphi_{ts}^{(3)} &= A_{ts}^{(3)} e^{i(\omega t - \mathbf{q}_{ts}^{(3)}\cdot\mathbf{x})},\\
\psi_{tc}^{(3)} &= B_{tI}^{(3)} e^{i(\omega t - \mathbf{q}_{tI}^{(3)}\cdot\mathbf{x})} + B_{tII}^{(3)} e^{i(\omega t - \mathbf{q}_{tII}^{(3)}\cdot\mathbf{x})},\\
\psi_{ts}^{(3)} &= B_{ts}^{(3)} e^{i(\omega t - \mathbf{q}_{ts}^{(3)}\cdot\mathbf{x})}.
\end{aligned} \tag{A3}$$

In general, the wave vectors can be written as

$$\mathbf{q}_{lj} = (\chi_{lj}, \beta_{lj}) = q_{lj}(\pm\sin(\theta_{lj}), \cos(\theta_{lj})), \tag{A4}$$

with l indicating the kind of events and j indicating the waves. The positive sign is for the incident and transmitted waves, and the negative sign is for the reflected waves.

The solid and relative fluid displacements $U^{(n)} = (U_x^{(n)}, U_z^{(n)})$ and $W^{(n)} = (W_x^{(n)}, W_z^{(n)})$, in the three different media, are given by (Santos *et al.* 1992),

$$\begin{aligned}
U^{(1)} &= \nabla\varphi_{iI} + \nabla\varphi_{rc}^{(1)} + \left(-\frac{\partial\varphi_{rs}^{(1)}}{\partial z}, \frac{\partial\varphi_{rs}^{(1)}}{\partial x}\right)\\
&= U_{iI}^{(1)} + U_{rI}^{(1)} + U_{rII}^{(1)} + U_{rs}^{(1)},
\end{aligned} \tag{A5}$$

$$\begin{aligned}
W^{(1)} &= \nabla\psi_{iI} + \nabla\psi_{rc}^{(1)} + \left(-\frac{\partial\psi_{rs}^{(1)}}{\partial z}, \frac{\partial\psi_{rs}^{(1)}}{\partial x}\right)\\
&= W_{iI}^{(1)} + W_{rI}^{(1)} + W_{rII}^{(1)} + W_{rs}^{(1)},
\end{aligned} \tag{A6}$$

$$\begin{aligned}
U^{(2)} &= \nabla\varphi_{tc}^{(2)} + \left(-\frac{\partial\varphi_{ts}^{(2)}}{\partial z}, \frac{\partial\varphi_{ts}^{(2)}}{\partial x}\right) + \nabla\varphi_{rc}^{(2)} + \left(-\frac{\partial\varphi_{rs}^{(2)}}{\partial z}, \frac{\partial\varphi_{rs}^{(2)}}{\partial x}\right)\\
&= U_{tI}^{(2)} + U_{tII}^{(2)} + U_{ts}^{(2)} + U_{rI}^{(2)} + U_{rII}^{(2)} + U_{rs}^{(2)},
\end{aligned} \tag{A7}$$

$$\begin{aligned}
W^{(2)} &= \nabla\psi_{tc}^{(2)} + \left(-\frac{\partial\psi_{ts}^{(2)}}{\partial z}, \frac{\partial\psi_{ts}^{(2)}}{\partial x}\right) + \nabla\psi_{rc}^{(2)} + \left(-\frac{\partial\psi_{rs}^{(2)}}{\partial z}, \frac{\partial\psi_{rs}^{(2)}}{\partial x}\right)\\
&= W_{tI}^{(2)} + W_{tII}^{(2)} + W_{ts}^{(2)} + W_{rI}^{(2)} + W_{rII}^{(2)} + W_{rs}^{(2)},
\end{aligned} \tag{A8}$$

$$U^{(3)} = \nabla\varphi_{tc}^{(3)} + \left(-\frac{\partial\varphi_{ts}^{(3)}}{\partial z}, \frac{\partial\varphi_{ts}^{(3)}}{\partial x}\right) = U_{tI}^{(3)} + U_{tII}^{(3)} + U_{ts}^{(3)}, \tag{A9}$$

and

$$W^{(3)} = \nabla\psi_{rc}^{(3)} + \left(-\frac{\partial\psi_{rs}^{(3)}}{\partial z}, \frac{\partial\psi_{rs}^{(3)}}{\partial x}\right) = W_{tI}^{(3)} + W_{tII}^{(3)} + W_{ts}^{(3)}. \tag{A10}$$

We impose the conditions

$$U_x^{(n)} = U_x^{(n+1)}, \tag{A11}$$

$$U_z^{(n)} = U_z^{(n+1)}, \tag{A12}$$

$$\sigma_{zz}^{(n)} = \sigma_{zz}^{(n+1)}, \tag{A13}$$

$$\sigma_{xz}^{(n)} = \sigma_{xz}^{(n+1)}, \tag{A14}$$

$$P_f^{(n)} = P_f^{(n+1)}, \tag{A15}$$

$$W_z^{(n)} = W_z^{(n+1)}, \quad n = 1, 2. \tag{A16}$$

The amplitude of the reflection and transmission coefficients R and T for the poroelastic thin layer are defined as the ratio of the solid-displacement amplitude of the corresponding wave and that of the incident wave, i.e.,

$$R_j^{(1)} = \frac{A_{rj}^{(1)} q_{rj}^{(1)}}{A_{iI}^{(1)} q_{iI}^{(1)}}, \tag{A17}$$

and

$$T_j^{(3)} = \frac{A_{tj}^{(3)} q_{tj}^{(3)}}{A_{iI}^{(1)} q_{iI}^{(1)}}. \tag{A18}$$

Using equations (8)-(A3), to obtain expressions for each of the pairs, (A17) and (A18), mentioned above and substituting them in (4) leads us to the following relationships between the amplitudes of the solid, and the relative fluid amplitudes:

$$B_{lj}^{(n)} = \gamma_{lj}^{(n)} A_{lj}^{(n)}, \quad j = I, II, s, \quad l = r, t, \quad n = 1, 2, 3,$$
$$B_{iI} = \gamma_{iI} A_{iI}, \tag{A19}$$

with

$$\gamma_{rj}^{(n)} = \frac{\left[\rho_b^{(n)}\omega^2 - \left(q_{rj}^{(n)}\right)^2 H_c^{(n)}\right]}{\left[\left(q_{rj}^{(n)}\right)^2 D^{(n)} - \rho_f^{(n)}\omega^2\right]} \quad j = I, II \quad n = 1, 2, \tag{A20}$$

$$\gamma_{tj}^{(n)} = \frac{\left[\rho_b^{(n)}\omega^2 - \left(q_{tj}^{(n)}\right)^2 H_c^{(n)}\right]}{\left[\left(q_{tj}^{(n)}\right)^2 D^{(n)} - \rho_f^{(n)}\omega^2\right]} \quad j = I, II \quad n = 2, 3, \tag{A21}$$

$$\gamma_{rs}^{(n)} = \frac{\mu^{(n)}\left(q_{rs}^{(n)}\right)^2 - \rho_b^{(n)}\omega^2}{\rho_f^{(n)}\omega^2} \quad n = 1, 2, \tag{A22}$$

$$\gamma_{ts}^{(n)} = \frac{\mu^{(n)}\left(q_{ts}^{(n)}\right)^2 - \rho_b^{(n)}\omega^2}{\rho_f^{(n)}\omega^2} \quad n = 2, 3, \tag{A23}$$

and

$$\gamma_{iI}^{(1)} = \frac{\left[\rho_b^{(1)}\omega^2 - \left(q_{i1}^{(1)}\right)^2 H_c^{(1)}\right]}{\left[\left(q_{i1}^{(1)}\right)^2 D^{(1)} - \rho_f^{(1)}\omega^2\right]}. \tag{A24}$$

The boundary conditions (A11)–(A16) require that the phase factors at the interfaces $z = 0$ and $z = h$ are the same:

$$\chi_{i1} = \chi_{rI}^{(1)} = \chi_{rII}^{(1)} = \chi_{rs}^{(1)} = \chi_{tI}^{(2)} = \chi_{tII}^{(2)} = \chi_{ts}^{(2)} = \chi_{rI}^{(2)} = \chi_{rII}^{(2)} = \chi_{rs}^{(2)} = \chi_{tI}^{(3)} = \chi_{tII}^{(3)} = \chi_{ts}^{(3)} = \chi, \tag{A25}$$

which represents Snell's law and allows us to obtain the reflected and transmitted angles θ_{lj} for each type of wave as a function of the incidence angle θ_{iI}.

Application of the boundary conditions (A11)–(A16) and Snell's law (A25) at $z = 0$ and $z = h$ give two systems of linear equations in the unknowns A_{rI} ,A_{rII}, A_{rs}, A_{tI}, A_{tII}, and A_{ts} (see Martinez *et al.* (2014)). These two systems have coefficients depending on the wave numbers $q_{lj}^{(n)}$.

Set

$$C_{lj}^{(n)} = A_{lj}^{(n)}/A_{iI}, \ \ l = r, t, \ \ j = I, II, s, \ \ n = 1, 2, 3, \tag{A26}$$

and use the matrix notation of Carcione (Section 6.4. 2015) to relate the fields at $z = 0$ and $z = h$. Thus,

$$(\mathbf{A}_1 - \mathbf{B} * \mathbf{A}_3)\,\mathbf{r} = -\mathbf{i}_p, \tag{A27}$$

where $\mathbf{r} = (C_{rI}^{(1)}, C_{rII}^{(1)}, C_{rs}^{(1)}, C_{tI}^{(3)}, C_{tII}^{(3)}, C_{ts}^{(3)})^\top$, $\mathbf{i}_p = [-\chi, -\beta_{iI}^{(1)}, \zeta_{iI}^{(1)}, -2\mu^{(1)}\chi\beta_{iI}^{(1)}, \xi_{iI}^{(1)}, -\beta_{iI}^{(1)}\gamma_{iI}^{(1)}]^\top$, and $\mathbf{B} = \mathbf{T}(z = 0) * (\mathbf{T}(z = h))^{-1}$ that acts as a boundary condition. The system matrices in (A27) are explained by Martinez *et al.* (2014). Solving the system, the expressions of the R-T coefficients (9), are obtained.

APPENDIX B: BOUNDARY CONDITIONS ACROSS A FRACTURE

In this Appendix, we complete the Nakagawa and Schoenberg's equations offering explicitly the components of the matrix $\widetilde{\mathbf{Q}}_{YX}$ given in (12):

$$\widetilde{\mathbf{Q}}_{YX}(1,1) = -4\mu^{(2)}\left(\frac{\chi}{\omega}\right)^2\left(1-\frac{\mu^{(2)}}{H_c^{(2)}}\right) - \frac{\left(\rho_f^{(2)}\right)^2 - \rho_b^{(2)}\widetilde{\rho}^{(2)}}{\widetilde{\rho}^{(2)}} - 2\mu^{(2)}\widetilde{B}\widetilde{\beta}\left(\frac{\chi}{\omega}\right)^2\left(-\frac{\rho_f^{(2)}}{\widetilde{\rho}^{(2)}} + \alpha^{(2)}\frac{2\mu^{(2)}}{H_c^{(2)}}\right)\cdot(1-\Pi),$$

$$\widetilde{\mathbf{Q}}_{YX}(1,2) = \frac{\chi}{\omega}\left[\left(1-\frac{2\mu^{(2)}}{H_c^{(2)}}\right) + \left(-\frac{\rho_f^{(2)}}{\widetilde{\rho}^{(2)}} + \alpha^{(2)}\frac{2\mu^{(2)}}{H_c^{(2)}}\right)\times\widetilde{B}\cdot(1-\Pi)\right],$$

$$\widetilde{\mathbf{Q}}_{YX}(1,3) = \frac{\chi}{\omega}\left(-\frac{\rho_f^{(2)}}{\widetilde{\rho}^{(2)}} + \alpha^{(2)}\frac{2\mu^{(2)}}{H_c^{(2)}}\right)\cdot\Pi,$$

$$\widetilde{\mathbf{Q}}_{YX}(2,1) = \frac{\chi}{\omega}\left(1-\frac{2\mu^{(2)}}{H_c^{(2)}} + 2\widetilde{B}\widetilde{\beta}\alpha^{(2)}\frac{\mu^{(2)}}{H_c^{(2)}}\cdot(1-\Pi)\right),$$

$$\widetilde{\mathbf{Q}}_{YX}(2,2) = \frac{1}{H_c^{(2)}} - \alpha^{(2)}\widetilde{B}\frac{1}{H_c^{(2)}}\cdot(1-\Pi),$$

$$\widetilde{\mathbf{Q}}_{YX}(2,3) = -\alpha^{(2)}\frac{1}{H_c^{(2)}}\cdot\Pi,$$

$$\widetilde{\mathbf{Q}}_{YX}(3,1) = \frac{\chi}{\omega}\left[-\frac{\rho_f^{(2)}}{\widetilde{\rho}^{(2)}} + \alpha^{(2)}\frac{2\mu^{(2)}}{H_c^{(2)}} - 2\widetilde{B}\widetilde{\beta}\left(\left(\alpha^{(2)}\right)^2\frac{\mu^{(2)}}{H_c^{(2)}} + \frac{\mu^{(2)}}{M^{(2)}} - \left(\frac{\chi}{\omega}\right)^2\frac{\mu^{(2)}}{\widetilde{\rho}^{(2)}}\right)\cdot(1-\Pi)\right],$$

$$\widetilde{\mathbf{Q}}_{YX}(3,2) = -\alpha^{(2)}\frac{1}{H_c^{(2)}} + \left(\left(\alpha^{(2)}\right)^2\frac{1}{H_c^{(2)}} + \frac{1}{M^{(2)}} - \left(\frac{\chi}{\omega}\right)^2\frac{1}{\widetilde{\rho}^{(2)}}\right)\widetilde{B}\cdot(1-\Pi),$$

$$\widetilde{\mathbf{Q}}_{YX}(3,3) = \left(\left(\alpha^{(2)}\right)^2\frac{1}{H_c^{(2)}} + \frac{1}{M^{(2)}} - \left(\frac{\chi}{\omega}\right)^2\frac{1}{\widetilde{\rho}^{(2)}}\right)\cdot\Pi. \tag{B1}$$

Furthermore, the explicit system of equations corresponding to (16) is

$$\begin{aligned}
&N_{1,1}A_{rI} + N_{1,2}A_{rII} + N_{1,3}A_{rs} + N_{1,4}e^{-i\beta_{tI}^{(3)}h}A_{tI} + N_{1,5}e^{-i\beta_{tII}^{(3)}h}A_{tII} + N_{1,6}e^{-i\beta_{ts}^{(3)}h}A_{ts} = i'_{p,1}A_{iI}\\
&N_{2,1}A_{rI} + N_{2,2}A_{rII} + N_{2,3}A_{rs} + N_{2,4}e^{-i\beta_{tI}^{(3)}h}A_{tI} + N_{2,5}e^{-i\beta_{tII}^{(3)}h}A_{tII} + N_{2,6}e^{-i\beta_{ts}^{(3)}h}A_{ts} = i'_{p,2}A_{iI}\\
&N_{3,1}A_{rI} + N_{3,2}A_{rII} + N_{3,3}A_{rs} + N_{3,4}e^{-i\beta_{tI}^{(3)}h}A_{tI} + N_{3,5}e^{-i\beta_{tII}^{(3)}h}A_{tII} + N_{3,6}e^{-i\beta_{ts}^{(3)}h}A_{ts} = i'_{p,3}A_{iI}\\
&N_{4,1}A_{rI} + N_{4,2}A_{rII} + N_{4,3}A_{rs} + N_{4,4}e^{-i\beta_{tI}^{(3)}h}A_{tI} + N_{4,5}e^{-i\beta_{tII}^{(3)}h}A_{tII} + N_{4,6}e^{-i\beta_{ts}^{(3)}h}A_{ts} = i'_{p,4}A_{iI}\\
&N_{5,1}A_{rI} + N_{5,2}A_{rII} + N_{5,3}A_{rs} + N_{5,4}e^{-i\beta_{tI}^{(3)}h}A_{tI} + N_{5,5}e^{-i\beta_{tII}^{(3)}h}A_{tII} + N_{5,6}e^{-i\beta_{ts}^{(3)}h}A_{ts} = i'_{p,5}A_{iI}\\
&N_{6,1}A_{rI} + N_{6,2}A_{rII} + N_{6,3}A_{rs} + N_{2,4}e^{-i\beta_{tI}^{(3)}h}A_{tI} + N_{6,5}e^{-i\beta_{tII}^{(3)}h}A_{tII} + N_{6,6}e^{-i\beta_{ts}^{(3)}h}A_{ts} = i'_{p,6}A_{iI}.
\end{aligned} \tag{B2}$$